



# Experimental study on the mechanical behavior and mesoscopic damage of Guiyang red clay during triaxial loading

Guosheng Yang<sup>1</sup> · Shuangying Zuo<sup>1,2</sup> · Daoyong Wu<sup>2</sup> · Yinting Huang<sup>1</sup> · Yabin Zhang<sup>1</sup> · Muwen Peng<sup>2</sup>

Received: 29 July 2021 / Accepted: 4 December 2021 / Published online: 14 December 2021  
© Saudi Society for Geosciences 2021

## Abstract

Red clay is a kind of regional residual clay formed through the physical and chemical weathering of carbonate rocks in a warm environment and under damp climate conditions. These clays have special physical and mechanical properties including a large void ratio, low compressibility, and good mechanical engineering properties. The exhausted saturation test, consolidated undrained shear test, and nuclear magnetic resonance test of red clay samples were conducted to reveal the evolution law of the pore structure and the effect of meso-damage on the mechanical behavior of Guiyang laterite during triaxial loading. The results show that the nuclear magnetic resonance T2 spectrum of Guiyang red clay under conventional triaxial loading mainly shows three peaks, and each single peak corresponds to a pore type. With the gradual application of load, the number of micro pores in red clay increases, and the radius decreases gradually at the meso level. The number of medium-large pores decreases, and the pore radius increases gradually. At the macro-level, the shear surface of red clay begins to form slowly and gradually develops to the stage of slip and compaction. The strength of the particles on the shear surface is gradually lost, and the deformation of soil becomes larger and larger. In addition, during the initial stage of shear, the shear strength of soil is mainly provided by its cohesive strength. With the gradual progress of shear, the cohesion will decrease, and the friction angle will increase, at which time the shear strengths will consist of cohesive strength and friction strength, respectively.

**Keywords** Guiyang red clay · Nuclear magnetic resonance · Pore structure · Plastic volumetric strain · Meso-damage

## Introduction

Red clay is widely distributed in the Yunnan-Guizhou Plateau, the adjacent central and western Guangxi, and western Hunan (China). In recent years, research has shown that red clay is a residual clay formed after the physical and chemical weathering of carbonate rocks in a warm environment, with a damp climate and abundant rainfall. Because of both the roles of the environment and different degrees of laterization, red clay in different places also differs markedly in its geological and engineering properties. Red clay which is

distributed in the central Guizhou Province is named Guiyang red clay and is characterized by a large void ratio, low compressibility, good mechanical properties, and a high bearing capacity (Liao and Zhu 2004). Red clay is an important part of the foundation materials and engineering fillers of highway subgrade, buildings, or structures; it is also one of the important material sources inducing geological disasters. Hu et al. (2004), Yang and Huang (2008), and Tang et al. (2013) carried out experimental research on the water content, shrinkage, and consistency of red clay by analyzing the parameters that mainly caused the strength of red clay to change, and pointing out the defects in the physical properties of red clay. For a period of time, scholars have scientifically evaluated the strength and deformation of red clays from the aspects of road traffic, housing construction, slope stability, and other engineering fields of red clay, and proposed mechanisms to improve red clays such as adding curing agents, which would optimize construction technology and change their foundation. This would help solve the adverse effects of the special engineering properties of red clay (Liang 2007; Tan et al. 2010; Yang and Yang 2012; Sun

Responsible Editor: Zeynal Abiddin Erguler

✉ Shuangying Zuo  
syzuo@gzu.edu.cn

<sup>1</sup> College of Resource and Environmental Engineering, Guizhou University, Guiyang 550025, China

<sup>2</sup> Key Laboratory of Karst Geological Resources and Environment, Ministry of Education, Guizhou University, Guiyang 550025, China

et al. 2013; Wei 2019). However, the macroscopic deformation and failure of red clay is essentially a concentrated reflection of the cumulative change of its meso-structure, and the change rule of the meso-structure is the internal mechanism of macroscopic mechanical behavior. With the continuous deepening of research, people began to gradually turn from the study of soil genesis, mineral composition, strength failure, and deformation mechanisms to the study of particle morphology, arrangement, and pore structure at the fine micro level, discussing the relationship between macro mechanical behavior and microstructure response (Li 2008; Roozbahani et al. 2017; Wang et al. 2018; Xu et al. 2020).

Due to the rapid development of advanced computer image processing techniques and 3D scanning technology, as well as the interplay of multiple disciplines, the study of porous media has become more in depth and is no longer limited by traditional methods and technical means. As a new type of rapid, non-destructive, and accurate detection method, nuclear magnetic resonance (NMR) technology provides technical support for the study of the meso-structure of geotechnical materials. The applicability and reliability of NMR technology in evaluating the water retention, permeability, pore structure, and water migration of porous media have been discussed in detail through a large number of laboratory tests (Jaeger et al. 2009; Costabel and Yaramanci 2011; Maurer and Knight 2016; Shi et al. 2017; Kong et al. 2017; Zheng et al. 2018). At present, NMR technology has been widely used in porous media tests and research. Li et al. (2014) pointed out that the surface relaxation rate of samples can control their pore size but does not affect the percentage of each pore size in mucky soils. Tian et al. (2014) studied the migration and micro-dynamic behavior of water in compacted clays based on NMR technology. Finally, An and Liao (2018) pointed out that the change in soil pore structure is the internal reason for the development of strength and deformation.

In fact, the failure process of soil strength under loads can be regarded as a cumulative process of soil meso-damage behavior. In previous studies, damage models have been developed based on traditional test methods, classical elastic–plastic theory, strain equivalence principles, and complex theoretical derivations to better describe the stress–strain relationship in soils (Yao and Hou 2008; Hu et al. 2011; Zhang et al. 2017). Although this research idea has been used previously and will continue to be applicable for a certain period of time of the future, it is always based

on the research on macrophysics and mechanics, not the actual changes of soils' internal structures. NMR technology may provide some solutions. At present, the research on the strength and meso-damage behavior of red clays is still under exploration. Zhang et al. (2020) simulated different stress combinations through indoor triaxial tests and discussed the meso-damage mechanisms of red clay under load. Wang et al. (2020) used electron microscopy to study the variation of the mechanical properties of alkaline red clays after treatment and established a relationship between the shear strength parameters and microstructure parameters of alkaline red clays. Chen et al. (2021a, b) analyzed the filling and strengthening effects of lime on the pore structure of red clays by using low-field NMR technologies; the authors also discussed the effects of meso-structure changes on the strength of red clay. The results of these research outputs also provided ideas about studying meso-damage behavior and damage mechanisms of red clay. However, only the initial state of the red clay and the two states after final failure after loading have been studied, and the study on the whole of the shear processes of Guiyang red clay is insufficient. Therefore, this paper considers the Guiyang red clays and discusses the meso-structure response of red clays under load by investigating the changes in pore number, pore size distribution, and porosity for the same sample throughout the shearing process by triaxial compression tests and low-field NMR techniques. Moreover, the Mohr–Coulomb strength theory was combined to analyze the evolution of cohesion and internal friction angle during the whole shear process and to elucidate the strength and deformation characteristics of the red clays during the whole loading process.

## Material and methods

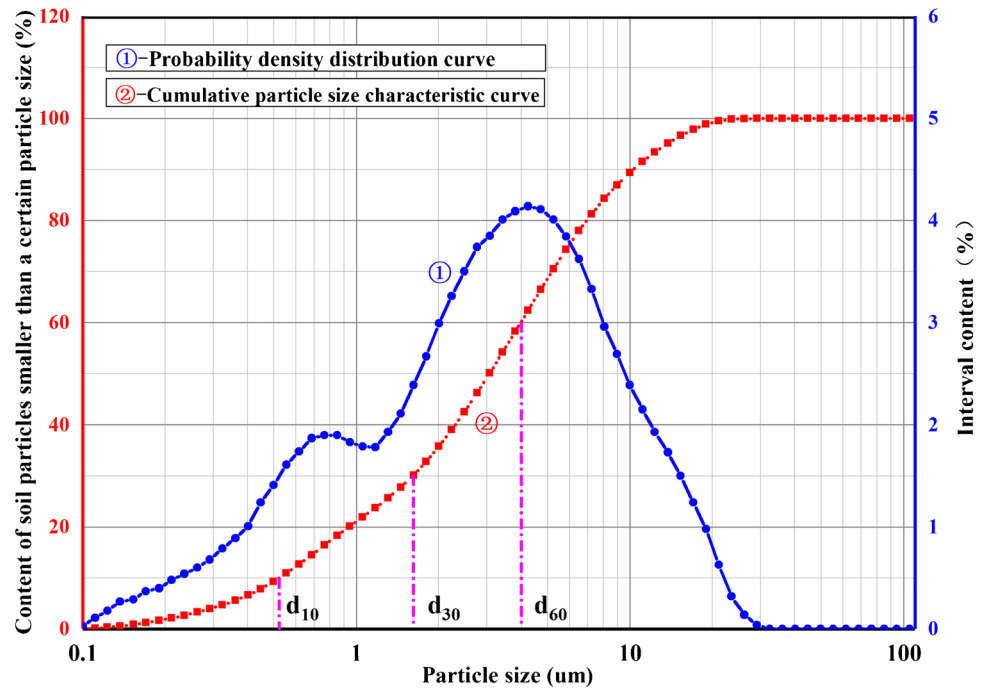
### Sample preparation

The red clay samples were taken from the geophysical exploration test site in Guizhou University, with a depth of 3–5 m. The soil is brown-yellow, in hard-plastic states, with a dense structure and uniform texture. The sample consists of quartz, muscovite, staurolite, and other minor minerals. The fundamental physical and mechanical parameters of red clays are shown in Table 1. The particle size distribution curve of the test for red clay was obtained with a laser particle size analyzer (Zuo et al. 2018). As shown in Fig. 1.

**Table 1** Fundamental physical and mechanical indices of Guiyang red clay

Natural moisture content/ $\omega$ (%)	Wet density/(g/cm <sup>3</sup> )	Gravity/ $G_s$	Liquid limit/ $\omega_L$ (%)	Plastic limit/ $\omega_p$ (%)	Plasticity index/ $I_p$	Liquidity index/ $I_L$	Void ratio/ $e$
32.94	1.736	2.647	48.18	30.59	17.59	0.14	1.03

**Fig. 1** Compaction curve of Guiyang red clay



The curvature of the coefficient  $C_c = 0.85$  and the inhomogeneity coefficient  $C_u = 6.77$  of the test soil sample indicate poor grading. The probability density distribution curve shows a bimodal type, indicating that some particle sizes of the test soil samples are missing. According to the geotechnical engineering investigation specification (MCPRC MCPRC 2001), the soil samples are classified, and the test soil samples are cohesive soil in hard plastic state. According to a national standard of the Chinese geotechnical test method (MWRPRC 2019), the sample preparation was carried out according to the following process. Firstly, several soil blocks with sizes of at least  $200 \times 150 \times 150$  mm were taken from the geophysical exploration test field. Secondly, the soil block is carefully winged by the cutter to make the soil block with the size of about  $150 \times 50 \times 50$  mm. Then, the surface of the red clay test block was smoothed repeatedly by using a common soil cutting disc and steel wire saw in the laboratory geotechnical test, producing a cylindrical sample of about  $\phi 39.1 \times 120$  mm in size. Finally, the cylindrical sample was loaded into the standard die with an inner diameter of  $\phi 39.1 \times 80$  mm. The excess soil samples at both ends of the cylindrical sample were then lightly removed with a soil cutter to make the standard sample of  $\phi 39.1 \times 80$  mm.

### Exhausted saturation test

When using low-field NMR technology to test the pore index of soil, the hydrated state of red clay samples can greatly influence the test results due to its low permeability. A triaxial saturation device and vacuum pumping equipment were

adopted to exhaust and saturate the sample to make the red clay sample reach its saturation state (Fig. 2a). Two groups of saturation tests on the same red clay sample before and after the damage were conducted to discuss and analyze the changes in pore structure during loading. According to the Chinese standard for soil test methods, the saturation test on the test soil sample should follow the following process:

1. The sample should be loaded into a three-axis saturated device
2. The saturator should be put into the saturated cylinder and the saturated cylinder; should be sealed
3. The open-air extraction should switch between the vacuum cylinder and the air extractor, in order to prompt the air extractor to start extracting (the air extraction time shall not be less than 1 h)
4. Keeping the negative pressure in the saturated cylinder unchanged, open the water inlet switch, so that the water will slowly flow into the saturated cylinder to submerge the saturator; close the switch; this way, the specimen becomes fully saturated after 10 h

The saturated moisture content of the soil was measured by controlling the time of gas extraction and saturation. Combined with Eq. (1), the saturation of red clay under different saturation states was calculated. After the exploration and practice of the preliminary test, due to the special low permeability material of red clays, the latter requires 3 h of air extraction time and 9 h of saturation time to make the sample fully saturated and meet the requirements of the test.

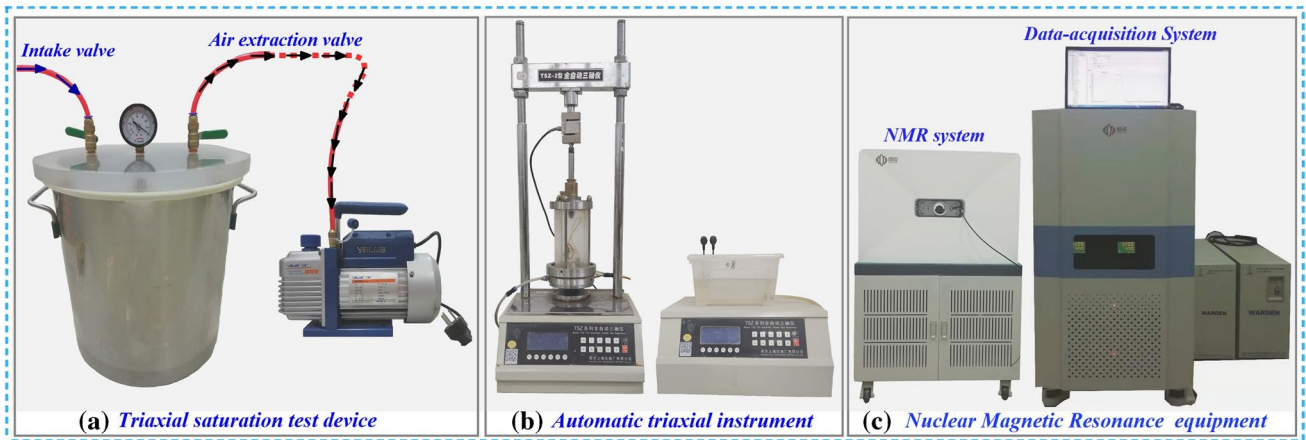


Fig. 2 The test equipment and devices

It should be pointed out that the specimen will deform after damage, which will make it difficult to saturate again. The specimen must then be preprocessed again (Fig. 3):

$$S_r = \frac{\omega_{sr} G_s}{e} \quad (1)$$

where  $\omega_{sr}$  is the water content of the specimen after saturation,  $G_s$  is the specific gravity of the soil particles,  $e$  is the void ratio of the specimen, and  $S_r$  is the saturation of the specimen.

### Triaxial test

A fully automated triaxial apparatus with TSZ-2 produced by Nanjing Soil Instrument Factory Co., Ltd. was used in the test (Fig. 2b). Because moisture content greatly influences the mechanical strength of the soil, the saturated sample after the initial NMR test was naturally dehydrated at indoor temperatures. The mass  $m_i$  of the sample was measured in real time until the error range between  $m_i$  and the initial sample mass  $m_0$  was within 0.2 g. Then, the consolidated undrained shear triaxial tests of the red clay samples with

different confining pressures were carried out. The confining pressures were set at 100 kPa, 150 kPa, 200 kPa, and 300 kPa, and the consolidation process was terminated by the dissipation of pore water pressure to 0. The shear process was carried out by keeping the confining pressure constant and controlling the shear rate at 0.008 mm/min by applying some axial stress. If  $\epsilon_1 \geq 3\%$ , the deformation of the sample will be mainly plastic deformation and less elastic deformation. At this time, the pore structure of the sample will be gradually fixed and will not recover. Therefore, this paper indirectly investigates the meso-damage behavior of red clay soils throughout the shear process under conventional loading by using  $\epsilon_1 = 3\%$  as the initial strain point, with a spacing of 3%, and controlling  $\epsilon_1$  at 3%, 6%, 9%, 12%, 15%, and 18% as the test end conditions. It should be noted that all analysis results are only applicable within the set confining pressure range. There were 24 samples in the test, and the test scheme is shown in Table 2.

### Low-field NMR test

A MesoMR12-060H-I-type nuclear magnetic resonance imaging analyzer produced by Suzhou Niumag Analytical



Fig. 3 Specimens pretreatment under different degrees of damage

**Table 2** Test scheme of the meso-damage behavior of Guiyang red clay under load

$\sigma_3$ (kPa)	$\epsilon_1 = 3\%$	$\epsilon_1 = 6\%$	$\epsilon_1 = 9\%$	$\epsilon_1 = 12\%$	$\epsilon_1 = 15\%$	$\epsilon_1 = 18\%$
100	1 <sup>#</sup>	2 <sup>#</sup>	3 <sup>#</sup>	4 <sup>#</sup>	5 <sup>#</sup>	6 <sup>#</sup>
150	7 <sup>#</sup>	8 <sup>#</sup>	9 <sup>#</sup>	10 <sup>#</sup>	11 <sup>#</sup>	12 <sup>#</sup>
200	13 <sup>#</sup>	14 <sup>#</sup>	15 <sup>#</sup>	16 <sup>#</sup>	17 <sup>#</sup>	18 <sup>#</sup>
300	19 <sup>#</sup>	20 <sup>#</sup>	21 <sup>#</sup>	22 <sup>#</sup>	23 <sup>#</sup>	24 <sup>#</sup>

Instrument Corporation was used in the test, with a magnet temperature of  $32 \pm 0.01$  °C, RF center frequency of 12 MHz, and RF offset frequency of 645.55671 kHz. The test instrument and main parameters are shown in Fig. 2c and Table 3. NMR technology studies the properties of fluids in geotechnical materials by measuring hydrogen nuclei with the spin ability. It also generally uses the transverse relaxation time T2 to characterize pore fluids. The relaxation time of fluids can be divided into volume relaxation, surface relaxation, and diffusion relaxation. Because the sample is in a uniform magnetic field, the volume relaxation and diffusion relaxation of the soil can be ignored. Therefore, the transverse relaxation time can be expressed as the following Eq. (2):

$$\frac{1}{T_2} \approx \frac{1}{T_{2s}} = \rho_2 \left( \frac{S}{V} \right)_{\text{pore}} = \rho_2 \frac{F_s}{r} \tag{2}$$

The transverse surface relaxation rate  $\rho_2$  is related to the pore surface and cementation properties of materials (Liu et al. 2011).  $T_{2s}$  is the surface relaxation time;  $(S/V)_{\text{pore}}$  is the pore structure parameter, which is the ratio of the pore surface area to the pore volume, abbreviated as the specific surface area of the pore;  $F_s$  is the pore shape factor; when the pore is assumed to be cylindrical,  $F_s = 2$ ; when the pore is spherical,  $F_s = 3$  (Godefroy et al. 2001). In this paper, the pore volume of red clay is considered to be spherical. Previous research on red clays based on NMR technology has shown that the transverse surface relaxation rate of red clay is 3.0  $\mu\text{m/s}$  (Chen et al. 2021a, b). Combining with Eq. (2), it can be seen that the pore size of the sample has a linear relationship with the transverse relaxation time  $T_2$ . The value of the transverse surface relaxation rate is only the amplification or reduction factor of the pore radius of the sample. It does not affect the pore size distribution of the macropores, mesopores, and small pores in the sample.

**Test implementation**

The tests mainly included the following steps. First, the original samples were prepared according to the specification

requirements, and then the first saturation tests were carried out using a triaxial saturation device. Secondly, the saturated samples were tested using a low-field NMR technology. Thirdly, the saturated red clay samples were placed at indoor temperatures to lose their water until the mass error ranged between the saturated samples, and the corresponding initial samples were within 0.2 g. Fourthly, triaxial consolidation undrained shear tests were carried out on the partially dehydrated samples. When the deformation of the samples reached the setting deformation condition ( $\epsilon_1 = 3\%, 6\%, 9\%, 12\%, 15\%$ , and  $18\%$ ), the test was stopped. Lastly, the sample that was damaged by loading was taken out to be saturated, and the pore structure was tested with NMR technology.

**Results and analysis**

**Stress–strain relationship and T2 spectrum distribution characteristics**

Triaxial compression tests were carried out to study the mechanical properties and pore evolution of Guiyang red clay at confining pressures of 100 kPa, 150 kPa, 200 kPa, and 300 kPa. The experimental results of each group are very similar. This paper only takes the confining pressure  $\sigma_3 = 150$  kPa as an example for discussion and analysis. Figure 4 shows the stress–strain relationship curves of the triaxial compression tests at the end of  $\epsilon_1 = 3\%, 6\%, 9\%, 12\%, 15\%$ , and  $18\%$  with the confining pressure of 150 kPa. It can be seen that the changing trends of the stress–strain curves of the tests are the same and show hardened-strain characteristics. Furthermore, in the range of  $\epsilon_1 = 0\text{--}2\%$  of minor strain, the stress–strain relationship curves rise sharply, the strain increments of the sample are smaller, and the principal stress changes significantly. When the deformation of the samples exceeds  $\epsilon_1 = 2\%$ , the curves begin to flatten gradually, and the strain of the samples changes considerably, while the change of principal stress is not substantial. This process can be regarded as the beginning of the gradual penetration of the shear surface. On a micro-level, the porosity of the sample decreases, the sliding occurs

**Table 3** Main parameters of the low field NMR test

P90 ( $\mu\text{s}$ )	P180 ( $\mu\text{s}$ )	RG <sub>1</sub> (dB)	RG <sub>2</sub>	Forward shift	TR (ms)	NS	Echo time ( $\mu\text{m}$ )	NECH
8.52	16.48	10	3	1	3000	32	0.15	12,000

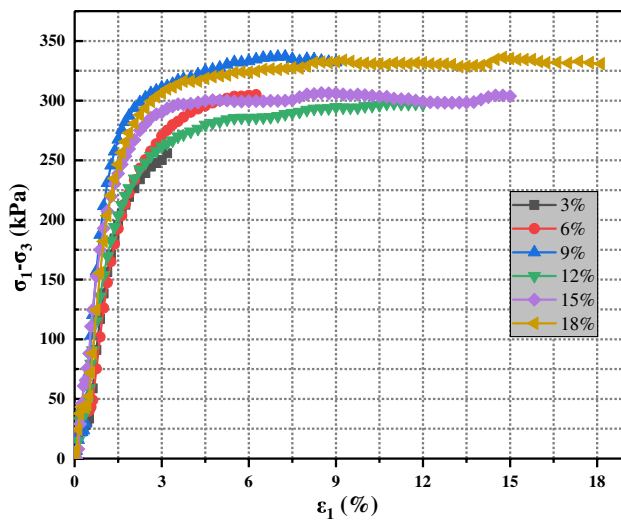


**Fig. 4** Stress–strain relationship curves of Guiyang red clay under different strains

between particles, and thus, the amount of damage to the sample is gradually strengthened.

The number of NMR signals represents the number of hydrogen nuclei in the sample and reflects the porosity of geotechnical materials (Jaeger et al. 2009). The NMR T<sub>2</sub> spectra of Guiyang red clays mainly exhibit a “three-peak pattern,” with the first, second, and third peaks ranging from 0.3 to 5 ms, 11 to 100 ms, and 100 to 3000 ms, respectively (Fig. 5). Combined with the analysis of Eq. (2), the range of the first peak corresponds to the small pores of the specimen, and the range of the second and third peaks corresponds to the medium-large pores of the specimen. The NMR T<sub>2</sub> spectra of the whole shear process of Guiyang red clays were analyzed, and it was found that the NMR T<sub>2</sub> spectra of the damaged red clay generally moved to the right side of the coordinate axis. The movement of the first peak was small, and the movements of the second and third peaks were large. Moreover, the signal amount of the first peak increased, and the signal amount of the other two peaks decreased, indicating that the increase in the pore size of the small pores of the sample was not obvious, and the increase in the radius of the medium-large pores was more obvious. The number of small pores in the sample gradually increased, and the number of large pores gradually decreased. This reveals the variation of pore sizes in red clays under conventional triaxial loading. It should be noted that when the strain reaches 15%, the variation of the NMR T<sub>2</sub> spectra of Guiyang red clays before and after shear is the largest, indicating that the number of small pores and the pore size of medium-large pores of the sample have reached their maximum. At this time, the sample has formed a shear failure surface, and the sample has been damaged. With the continuous development of the strength damage of red clay, the signal and movement quantities of

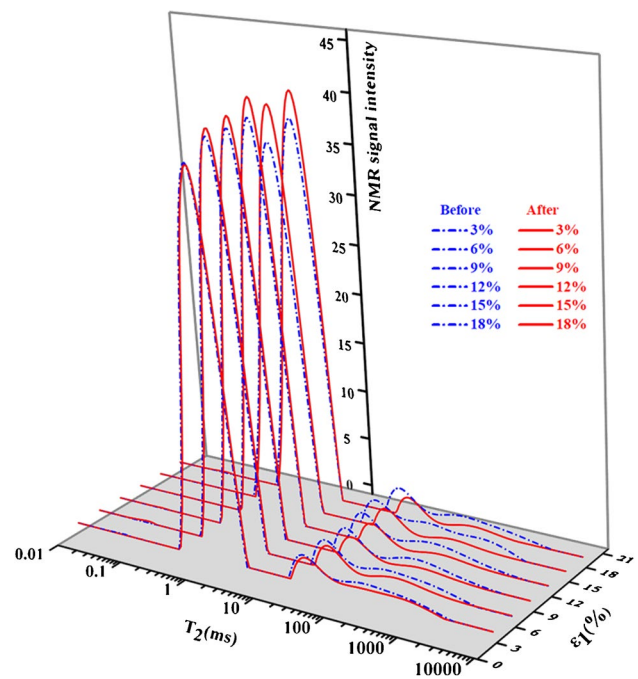


**Fig. 5** NMR relaxation curves before (blue) and after (red) injury

the three peaks of the nuclear magnetic resonance T<sub>2</sub> spectra of red clays begin to decrease again. At this time, the number of small pores and the pore diameter of medium-large pores begin to decrease again, caused by the sliding of the sample along the shear plane and the compaction of the pores on the shear plane.

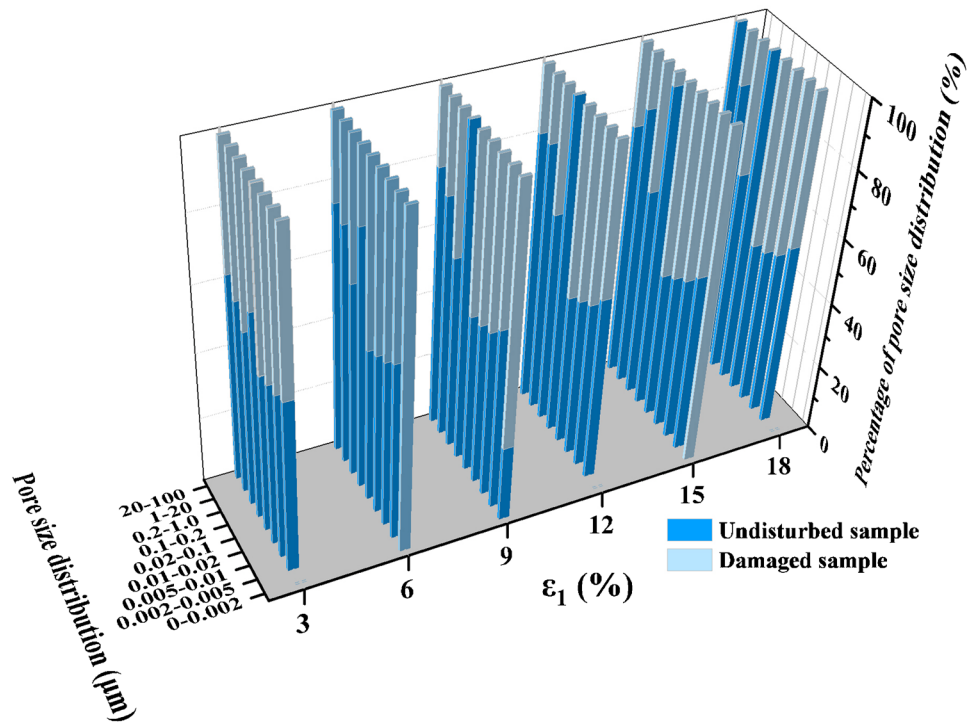
### Pore size distribution characteristics

As mentioned above, the pore types of red clay specimens can be broadly classified into three types: small, medium, and large pores, based on the “triple-peaked” pore structures exhibited by the red clay. As shown in Fig. 6, if the pore radius  $r \leq 0.1 \mu\text{m}$ , it is a small pore, pore radii within the range of 0.1 to  $\sim 1 \mu\text{m}$  characterize medium pore, and if pore radii  $r > 1 \mu\text{m}$ , the pores are large. Under the continuous action of stress, the percentage of small pores in the red clay specimen after shearing showed an increasing trend, and the percentage of large-medium pores showed a decreasing trend, but the pore size distribution of large-medium pores in the red clay showed the largest amount of change, which confirmed that the application of load mainly changed the radius of large-medium pores in the red clay and induced a gradual development of large-medium pores to small pores.

### Pore evolution law during loading

Many research results have shown that the porosity of porous media can be measured using low-field NMR technology,

**Fig. 6** Pore size distributions of undisturbed and damaged samples



displaying a high reliability (Li et al. 2017; Xie et al. 2018; Zhu et al. 2019). Six groups of triaxial compression tests with different strains were carried out under four different confining pressures. The pore volumes of 24 red clay samples before and after damage were statistically analyzed using low-field NMR technology, and the step-by-step increment of pore volumes under different strain conditions was obtained. Since the initial volume of the standard triaxial sample  $V_0 = 96.058$  ml, the average pore volume of 24 samples before damage  $V_a = 51.78$  ml was taken as the initial value. It is assumed that the red clay particles are incompressible, and only slip dislocation occurs between particles. The variation law of the pore volume of Guiyang red clay during the whole shear process can be obtained. The evolution law of porosity and void ratio during the shear process was deduced and calculated when the confining pressure was 150 kPa (Table 4). Figure 7 shows the evolution process of porosity during the damage process of Guiyang red clays

under four different confining pressures. It can be seen that with the gradual increase of strain, the porosity decreases as a whole during the first phase. Until the strain  $\epsilon_1$  reached 6%, the porosity of the damaged samples decreased to the minimum value, then began to increase. After that, the internal pores of the samples began to expand, extend, connect, and generate new tiny pores until the strain reached 15%. A macroscopic shear failure surface was formed in the soil, finally slipping, and compaction occurred on the shear failure surface. At the same time, it can be seen from Fig. 7 that the greater the confining pressure, the smaller the change of porosity of damaged samples, and the confining pressure had a restrictive effect on the pore volume of the samples.

**Shear strength parameters**

The triaxial compression test results of the Guiyang red clays with  $\sigma_3 = 100$  kPa, 200 kPa, 300 kPa at  $\epsilon_1 = 18\%$  were

**Table 4** Pore volume variation of Guiyang red clays at 150 kPa

$\epsilon_1$	Sample volume (ml)	Pore volume (ml)	Porosity (%)	Particle volume (ml)	Void ratio
0	96.058	51.77545	53.90019	44.2825539	1.169206
3	94.61761029	50.33506	53.1984	44.2825539	1.136679
6	94.31358672	50.03103	53.04753	44.2825539	1.129814
9	94.82307835	50.54052	53.29981	44.2825539	1.141319
12	94.33308649	50.05053	53.05724	44.2825539	1.130254
15	95.11672766	50.83417	53.44399	44.2825539	1.14795
18	94.51117803	50.22862	53.1457	44.2825539	1.134276

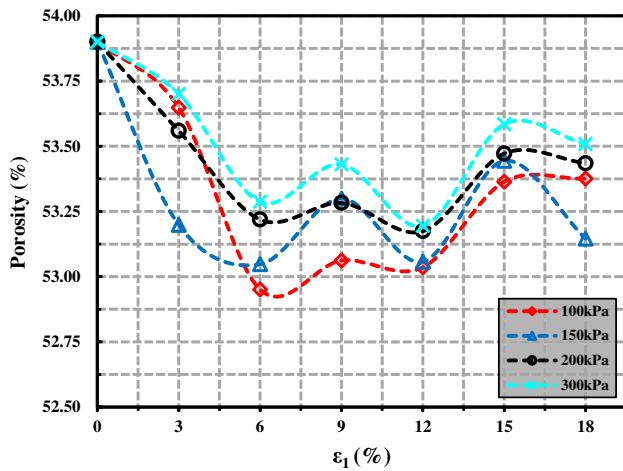
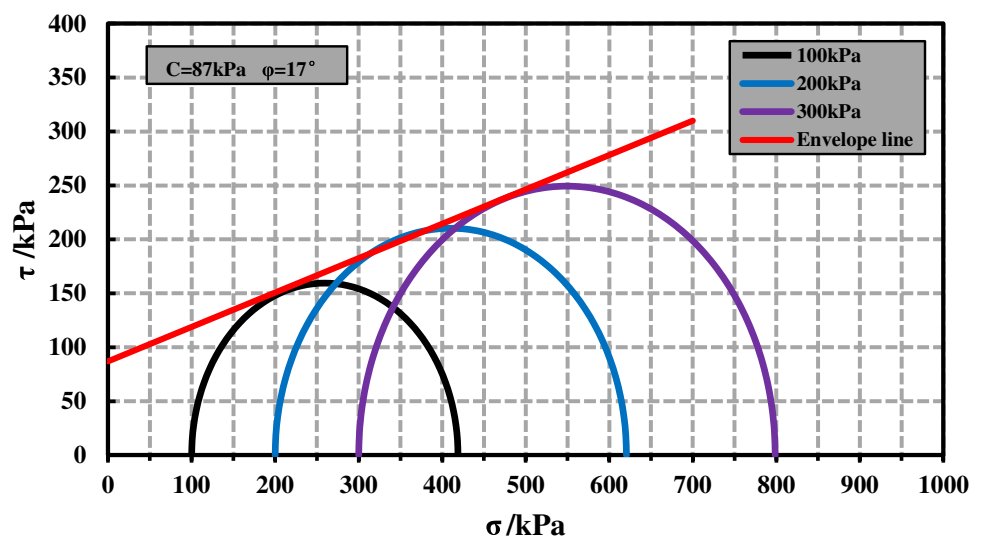


Fig. 7 Variations of porosity in shearing process under different confining pressures

analyzed. There is no obvious peak point in the stress–strain curve of the sample, so the principal stress difference corresponding to  $\epsilon_1 = 15\%$  was taken as the failure point according to the standard of a geotechnical test method. The breakdown stress circle was drawn with the shear stress as the ordinate and the normal stress as the abscissa (Fig. 8). The two shear strength parameters of red clay samples were  $c = 87$  kPa with an internal friction angle  $\varphi = 17^\circ$ . The red clay samples in the test showed strain hardening and no obvious softening deformation. The residual strength of the red clays was taken as the corresponding stress value of  $\epsilon_1 = 18\%$ . The residual shear strength parameters of the sample were obtained with the same method as above, with a residual cohesion  $c' = 78$  kPa and a residual internal friction angle  $\varphi' = 19^\circ$ .

Fig. 8 Shear strength parameters of Guiyang red clay



## Meso-damage behaviors of Guiyang red clays

### Plastic volumetric strain

The deformation of geotechnical materials under loads can be divided into elastic deformation and plastic deformation. In previous studies, it was considered that the plastic volume strain is the sum of three directions of strain, that is,  $\epsilon_v = \epsilon_1 + \epsilon_2 + \epsilon_3$ , which is only of general significance and does not represent the actual volume strain. As mentioned above, the void ratio of red clays during the shear failure process under a confining pressure of 150 kPa was obtained (Table 4). However, the pore ratio obtained here no longer undergoes elastic deformation, but only plastic deformation after the spring-back from the sample deformation, which is essentially the plastic volumetric strain  $\epsilon_v^p$ . Therefore, the plastic volumetric strain of the sample can be expressed as Eq. (3):

$$\epsilon_v^p = \frac{e_0 - e_i}{1 + e_0} = \frac{\Delta e}{1 + e_0} \quad (3)$$

where  $\epsilon_v^p$  is the plastic volumetric strain,  $e_0$  is the initial void ratio,  $e_i$  is the deformation of, and  $\epsilon_i$  is the void ratio after unloading and spring-back.

### Mohr–Coulomb strength criterion

For many years, the Mohr–Coulomb strength criterion has been able to accurately express geotechnical strength and deformation characteristics under load, which are simple to calculate, with few parameters and a clear physical significance. Therefore, the Mohr–Coulomb strength criterion has been widely used in scientific research and engineering



practices of geotechnical materials. The Mohr Coulomb criterion holds the strength of geotechnical materials comprising cohesive and frictional strength, and it is shown in the following Eq. (4). The indoor triaxial compression test for Guiyang red clay was thus carried out ( $\sigma_1 \geq \sigma_2 = \sigma_3$ ); Eq. (4) can be further written as Eq. (5):

$$\tau_n = c + \sigma_n \tan \varphi \tag{4}$$

$$\sigma_1 = \sigma_3 \tan^2\left(\frac{\pi}{4} + \frac{\varphi}{2}\right) + 2c \tan\left(\frac{\pi}{4} + \frac{\varphi}{2}\right) \tag{5}$$

### Evolution of cohesion strength and internal friction angle during loading

During loading, the cohesive strength and frictional strength of rock and soil materials are also constantly changing. It is generally believed that in the small strain range, the load of geotechnical materials is mainly borne by cohesive strength. When the strain exceeds a specific range, the load will be jointly borne by cohesive strength and friction strength. In the extensive strain range, the strength of geotechnical materials is mainly provided by friction strength (Wang et al. 2012; Chen et al. 2021a, b). Rafiei Renani and Martin (2018) carried out a uniaxial compression test and triaxial cyclic loading and unloading tests of rocks. He reported the evolution law of rock cohesion and the internal friction angle with plastic strain, establishing the relationship between cohesion and the internal friction angle with plastic strain, as shown in Eqs. (6) and (7):

$$c = c_r + (c_i - c_r) \left[ 2 - \frac{2}{1 + \exp(-5 \frac{\epsilon_v^p}{\epsilon_r^p})} \right] \tag{6}$$

$$\varphi = \varphi_i + (\varphi_r - \varphi_i) \left[ \frac{2}{1 + \exp(-5 \frac{\epsilon_v^p}{\epsilon_r^p})} - 1 \right] \tag{7}$$

where  $c_i, c_r$  is the initial and residual cohesion.  $\varphi_i, \varphi_r$  is the initial and residual internal friction angle.  $\epsilon^p, \epsilon_r^p$  is the plastic strain and residual plastic strain.

The Mohr Coulomb strength criterion considers that when the stress ratio of a material reaches a particular limit value, the material will be destroyed, which can be regarded as the continuous decrease of material strength. Combined with the mechanical and deformation characteristics of the Guiyang red clays and the strength parameter values reported in previous research on red clay (Liao and Zhu 2004), it was assumed that the initial cohesion of the Guiyang red clays is 1.1 times that at failure, that the initial internal friction angle is 0, and the plastic volumetric strain

is taken as the residual plastic strain when the strain  $\epsilon_1 = 18\%$  under loading condition. Therefore, Eqs. (6) and (7) can be modified to Eqs. (8) and (9):

$$c = c_r + (1.1c_p - c_r) \left[ 2 - \frac{2}{1 + \exp(-5 \frac{\epsilon_v^p}{\epsilon_r^p})} \right] \tag{8}$$

$$\varphi = \varphi_r \left[ \frac{2}{1 + \exp(-5 \frac{\epsilon_v^p}{\epsilon_r^p})} - 1 \right] \tag{9}$$

where  $c_p$  refers to the cohesive force of the specimen as a failure.  $\epsilon_v^p$  refers to the plastic volumetric strain of the specimen under different axial strains.

By substituting the plastic volumetric strain obtained using NMR technology into Eqs. (8) and (9), the variation law of internal friction angle and cohesion of the Guiyang red clays under different stress variables at 150 kPa could further be obtained (Fig. 9). It can also be seen that the cohesion of the Guiyang red clay was gradually decreasing, showing a weakening effect, while the internal friction angle was gradually increasing, showing a reinforcement effect with the aggravation of damage.

### Inversion of the stress–strain relationship of Guiyang red clay under load

As mentioned above, the peak and residual shear strength parameters of Guiyang red clays and the void ratios of the samples under different confining pressures and strains were obtained through a series of laboratory experiments. Then, the plastic strain of the sample was also obtained. Combined

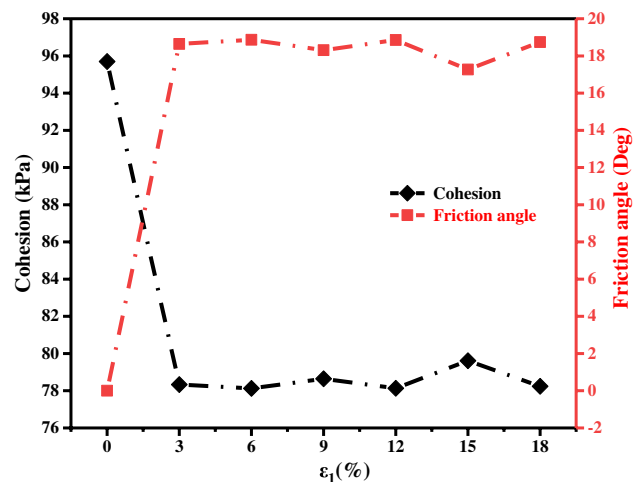


Fig. 9 Variations of internal friction angle and cohesion with axial strain

with Eqs. (8) and (9), the internal friction angle and cohesion corresponding to different strain variables of the sample under different confining pressures could be calculated. Finally, the different confining pressures were substituted into the triaxial compression case's Mohr–Coulomb strength criterion Eq. (5). Calculating the corresponding stress value  $\sigma_1$  under different deformations, the stress–strain relationship curve was drawn and compared with the stress–strain relationship curve under the indoor triaxial test (Fig. 10). It can be seen that the calculated values are in good agreement with the triaxial test curves, and the calculated values are slightly larger than the experimental values. The strength and deformation characteristics of the samples are also relatively consistent, which also indicates that it is scientific to indirectly obtain the plastic deformation of the damaged red clays by testing NMR technology.

## Discussion

1. The vacuum saturation test taken during the research may affect the internal pore structure of the soil and cause the loss of soil strength. Therefore, in this paper, the strength and deformation of saturated and unsaturated specimens were compared and analyzed by conducting control tests, and it was found that the trend of the stress–strain relationship curves of the two sets of test results was similar, and the peak strength of the soil only differed by about  $\pm 30$  kPa, which was the same as the difference in peak strength of different Guiyang red clay specimens (Fig. 4). We believe that this was caused by structural differences among the soil samples and was not related to the saturation test under ultimate negative pressures, which means that the effect of the vacuum saturation test on the structure and strength of the soil can be ignored.
2. In previous experimental studies of soil pore structure based on NMR technology, it has been difficult to test the same sample before and after damage, mainly because the specimen had been deformed and damaged after the force, producing the macroscopic form of soil change, and it was difficult to saturate the specimen, therefore making it impossible to apply NMR technology to test the pore structure. Indeed, the statistical law could only be derived through a large number of tests. In this paper, by pretreating the specimens with different degrees of damage (Fig. 3), the saturation of the damaged specimens was realized, and the pore structure change law of the Guiyang red clay specimens during the whole process of shearing was obtained indirectly, providing a worthy reference method for testing the pore structure change law of the specimens before and after damage under the action of load.

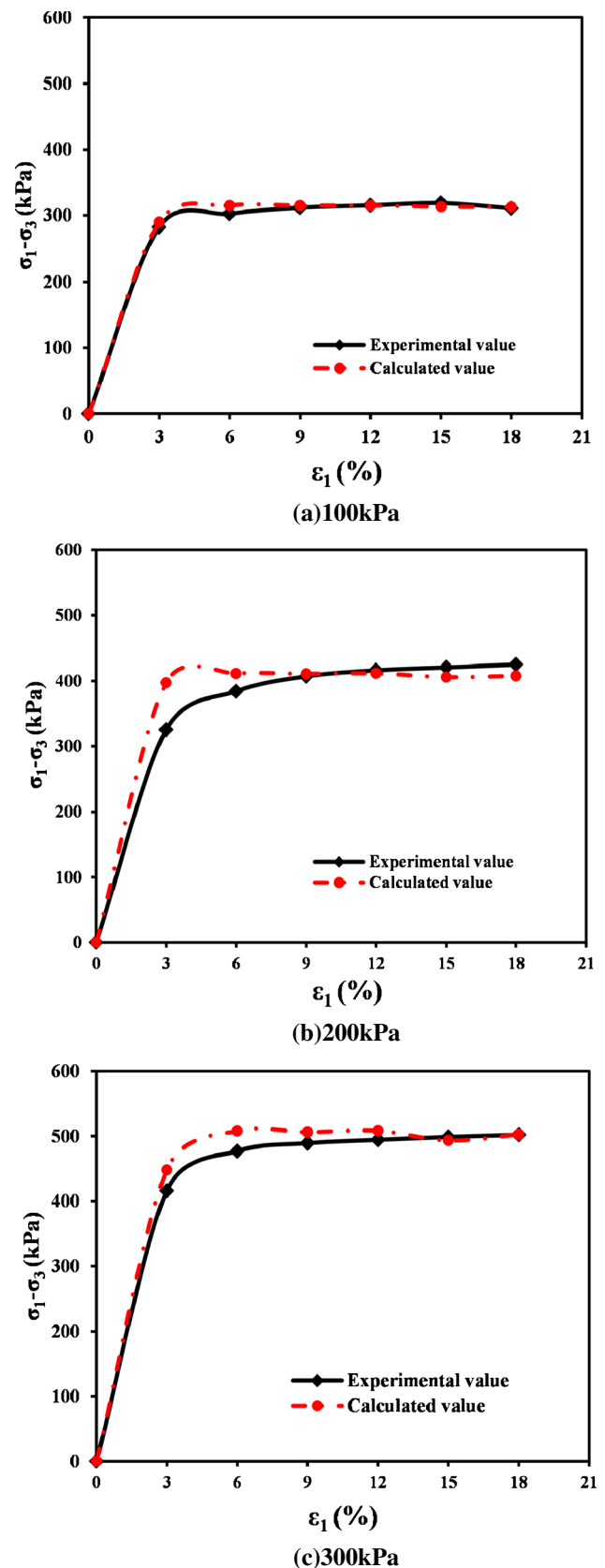


Fig. 10 Comparing between the calculated and experimental stress–strain curves of Guiyang red clay

3. Under the action of load, the damage of the soil gradually intensifies, and the overall porosity shows a trend of “decrease–increase–decrease,” indicating that the Guiyang red clays mainly exhibit pore volume compression under the condition of slight strain. After that, gradual loss of the connecting force between the particles, the soil particles began to slip and dislocate, showing the dilatancy deformation of the soil on the macro-level and the extension, expansion, connection, and generation of tiny pores on the micro-level. This led to the increase of the pore volume of the sample. After the shear surface is formed, the shear surface will slip and compact with the gradual application of stress, which will eventually cause the pore volume to decrease.
4. The volume of the sample in low-field NMR testing is a necessary parameter that determines the pore structure parameters. Although the volume of the specimen changes under loading conditions, the signal of the water content of the specimen obtained by NMR testing is always constant, and this part of the signal represents the pore volume of the specimen. The porosity of geotechnical materials is the ratio of the pore volume to the total volume of the specimen. Therefore, in this paper, the NMR test was carried out with the standard volume of the specimen (the actual volume of the sample was not exactly equal to 96.058 ml). It was then combined with the porosity obtained from the test. The pore volume of the specimen before and after the damage could be obtained, and the pore volume increment under all levels of strain calculates. Finally, the evolution law of the pore structure parameters of Guiyang red clay during the whole process of shear was obtained indirectly. The influence of the soil volume changes on the NMR test results during the shear process was neglected, and the plastic deformation of the soil under load could be evaluated more accurately.
5. Analysis from the inverse results of the stress–strain relationship curve verifies that the internal friction angle of Guiyang red clay gradually increases during the whole process of shear, while the cohesive force gradually decreases. Furthermore, the friction strength is strengthened, and the cohesive strength is weakened. Combining Eqs. (8) and (9), it could also be found that the plastic body strain of the specimen under load determines the strain hardening and strain softening of the specimen, while the initial cohesion and residual shear strength of Guiyang red clay affected the strength characteristics of the specimens. In addition, the stress–strain relationship of super consolidated red clay generally exhibits a strain-softening type behavior, and the residual strength of the specimen can be better obtained for this type of soil. For the Guiyang red clay, in turn, which exhibit strain-hardening type characteristics, the strength cor-

responding to the maximum strain of the specimen can be considered the residual strength of the specimen.

## Conclusions

In this paper, NMR technology was used to study red clay samples having undergone different degrees of damage, and indirectly obtaining the evolution law of pore sizes. Pore size distribution and porosity during the whole shear process of Guiyang red clay under triaxial load were identified, defining the plastic volume strain and exploring the mesoscopic damage behavior of Guiyang red clay. The NMR T2 spectrum chart of Guiyang red clays shows a “three-peak” pattern: there are three kinds of pores in the red clay, namely, tiny pores, medium pores, and large pores. During the whole shear process, the number of tiny pores increases, and the number of medium-large pores decreases. Moreover, the pore size distribution of large and medium pores is most sensitive to the change of stress state. Under the action of load, the overall change trend of porosity is “decreasing–increasing–decreasing,” which corresponds to the pore compaction stage, pore expansion, extension, connectivity, and new pore formation stage, as well as the slip compaction stage. At the same time, the confining pressure has a limiting effect on the porosity of the sample, and the larger the confining pressure, the smaller the change in porosity. The cohesive unit mainly provides strength at the beginning of the shear process, and load is applied gradually. The cohesive force will then be reduced, and the internal friction angle will increase, and the cohesive unit and friction unit will provide the strength of the sample. Guiyang red clay undergoing the shear process showed the cohesive strength’s weakening effect, and the friction strength showed the reinforcement effect.

**Funding** This work is supported by the National Natural Science Foundation of China (Grant Nos. 42167025, 42002280), the Science and Technology Foundation of Guizhou Province (Grant Nos. [2020]1Z052, [2019]1056), the first class subject foundation of Civil Engineering of Guizhou Province (QYNYL[2017]0013).

**Data availability** Some or all data, models, or code that support the findings of this study are available from the corresponding author upon reasonable request.

## Declarations

**Conflict of interest** The authors declare no competing interests.

## References

- An AJ, Liao JY (2018) Modified mesostructure of Standard Gange Railway expansive soils of Mombasa- Nairobi based on nuclear magnetic resonance and scanning electron microscope. Chin

- J Geo Eng. 40(+2): 151–156. <https://doi.org/10.11779/CJGE2018S2031>.
- Chen LJ, Chen XJ, Wang H, Huang X, Song Y (2021a) Mechanical properties and microstructure of lime-treated red clay. *KSCE J Civ Eng* 25:70–77. <https://doi.org/10.1007/S12205-020-0497-0>
- Chen SW, Liang F, Zuo SY, Wu DY (2021b) Evolution of deformation property and strength component mobilization for thermally treated Beishan granite under compression. *J Cent South Univ* 28:219–234. <https://doi.org/10.1007/s11771-021-4598-9>
- Costabel S, Yaramanci U (2011) Relative hydraulic conductivity and effective saturation from Earth's field nuclear magnetic resonance – a method for assessing the vadose zone. *Near Surf Geophys* 9(2):155–167. <https://doi.org/10.3997/1873-0604.2010055>
- Godefroy S, Korb JP, Fleury M, Bryant RG (2001) Surface nuclear magnetic relaxation and dynamics of water and oil in macroporous media. *Physical Review E*, 64: 021605/021601–021605/021613. <https://doi.org/10.1103/physreve.64.021605>
- Hu P, Huang MS, Ma SK, Lv XL (2011) A 3D Elastoplastic constitutive model for fine sand and its test verification. *Chin J Und Space Eng.* 7(04): 666–670+722. CNKI:SUN:BASE.0.2011-04-007.
- Hu SJ, Bi QT, Liao YL (2004) Influence of the “drying irreversibility” effect on the determination of liquid limit of red clay in Guizhou. *J Guizhou Univ Tech (Natural Science Edition)* (04):12–14+23. CNKI:SUN:GZGX.0.2004-04-004
- Jaeger F, Bowe S, Schaumann GE (2009) Evaluation of <sup>1</sup>H NMR relaxometry for the assessment of pore size distribution in soil samples. *Eur J Soil Sci* 60(6):1052–1064. <https://doi.org/10.1111/j.1365-2389.2009.01192.x>
- Kong LW, Sayem HM, Tian HH (2017) Influence of drying–wetting cycles on soil–water characteristic curve of undisturbed granite residual soils and microstructure mechanism by nuclear magnetic resonance (NMR) spin–spin relaxation time (T<sub>2</sub>) relaxometry. *Can Geotech J* 55(2):208–216. <https://doi.org/10.1139/cgj-2016-0614>
- Li JH (2008) A constitutive model of bonded soil based on the micro-mechanism of bonding-breakage. PhD dissertation. Tsinghua University.
- Li PF, Zhao XG, Guo Z, Ma LK, Chen L, Wang J (2017) Variation of strength parameters of Beishan granite under triaxial compression. *Chine J Rock Mech Eng.* 36(7):1599–1610. <https://doi.org/10.13722/j.cnki.jrme.2016.1412>
- Li ZM, Zeng WX, Gao ML, Luo ZB (2014) NMR experimental study on pore size distribution of silt under typical load conditions. *Acta Phys. Sin.* 63(5): 057401(1–7). <https://doi.org/10.7498/aps.63.057401>
- Liang Y (2007) Introduction to karst foundation design. *Coastal Enterprise and Technology* (10):144–145. CNKI:SUN:YQKJ.0.2007-10-052
- Liao YL, Zhu LJ (2004) Carboate laterite in Guizhou. Guiyang, China.
- Liu W, Xing L, Hao H, Sun W et al (2011) Nuclear magnetic resonance logging. Beijing, China.
- Maurer J, Knight R (2016) Models and methods for predicting hydraulic conductivity in near-surface unconsolidated sediments using nuclear magnetic resonance. *Geophysics* 81(5):D503–D518. <https://doi.org/10.1190/geo2015-0515.1>
- MCPRC (Ministry of Construction of the People's Republic of China) (2001) GB 50123–2001: Code for investigation of geotechnical engineering. MWRPRC, Beijing
- MWRPRC (Ministry of Water Resources of the People's Republic of China) (2019) GB/T 50123–2019: standard for soil test method. MWRPRC, Beijing
- Rafiei Renani H, Martin CD (2018) Cohesion degradation and friction mobilization in brittle failure of rocks. *Int J Rock Mech Min* 106:1–13. <https://doi.org/10.1016/j.ijrmms.2018.04.003>
- Roosbahani M, Borela R, Frost J (2017) Pore size distribution in granular material microstructure. *Materials*. 10(11): 1237–. <https://doi.org/10.3390/ma10111237>
- Shi FG, Zhang CZ, Zhang JB, Zhang XN, Yao J (2017) The changing pore size distribution of swelling and shrinking soil revealed by nuclear magnetic resonance relaxometry. *J Soils Sediments* 17(1):61–69. <https://doi.org/10.1007/s11368-016-1511-5>
- Sun CL, Guo AG, Tai J (2013) A comparative experimental study on lime modification of expansive soils and red clay. *Geotechnics (S2)*: 150–155. <https://doi.org/10.16285/j.rsm.2013.s2.072>.
- Tan YZ, Kong LW, Guo AG, Feng X, Wan Z (2010) Exploration of compaction control index for red clay roadbed filling. *Geotechnics (03)*: 851–855. <https://doi.org/10.16285/j.rsm.2010.03.021>.
- Tang W, Liao YL, Tang RX, Yi QB, Zhang YL (2013) Differences in the classification of consistency state index of red clay in Guizhou and its causes. *Hydrogeol Eng Geol* 40(05):81–86. <https://doi.org/10.16030/j.cnki.issn.1000-3665.2013.05.013>.
- Tian HH, Wei CF, Wei HZ, Yan RT, Chen P (2014) An NMR-based analysis of soil–water characteristics. *Appl Magn Reson* 45:49–61. <https://doi.org/10.1007/s00723-013-0496-0>
- Wang HC, Zhao WH, Sun DS, Guo BB (2012) Mohr-Coulomb yield criterion in rock plastic mechanics. *Chin J Geo* 55(12):4231–4238. <https://doi.org/10.6038/j.issn.001-5733.2012.034>
- Wang P, Qu Z, Charalampidou EM (2018) Shale hydration damage captured by nuclear magnetic resonance. *J Disper Sci Tech* 40(8):1–7. <https://doi.org/10.1080/01932691.2018.1496839>
- Wang Q, Chen J, Liu JK, Yu MY, Geng WJ, Wang PC, Wu ZG (2020) Relationships between shear strength parameters and microstructure of alkaline-contaminated red clay. *Environ Sci Pollut R.* 27(27). <https://doi.org/10.1007/s11356-020-09637-9>.
- Wei F (2019). Regional stability analysis of red clay slope based on different failure modes: a case study in Taizaihu Area, Fukuoka. *Adv Civ Eng.* <https://doi.org/10.1155/2019/1269832>
- Xie KN, Jiang DY, Sun ZG, Chen J, Zhang WG, and Jiang X (2018) NMR, MRI and AE statistical study of damage due to a low number of wetting–drying cycles in sandstone from the Three Gorges Reservoir Area. *Rock Mech Rock Eng.* 51(11). <https://doi.org/10.1007/s00603-018-1562-6>
- Xu J, Li Y, Ren C, Lan W (2020) Damage of saline intact loess after dry-wet and its interpretation based on SEM and NMR. *Soils Found.* 60(4). 10.1016/j.sandf.2020.06.006
- Yang DS, Huang QH (2008) Physical and mechanical properties and engineering characteristics of red clay in the Liupanshui area. *Shanxi Construction* 34(35):5–6. CNKI:SUN:JZSX.0.2008-35-004
- Yang X, Yang GL (2012) Red clay subgrade settlement calculation methods in Ballastless Track Design on high-speed railway. *Appl Mech Materials* 226–228:1571–1576. <https://doi.org/10.4028/www.scientific.net/amm.226-228.1571>
- Yao YP, Hou W (2008) A uniform hardening model for K<sub>0</sub> super-consolidated soils. *Journal of Geotechnical Engineering (03)*, 316–322. CNKI:SUN:YTGC.0.2008-03-002
- Zhang D, Liu EL, Liu XY, Zhang G, Yin X, Song BT (2017) A damage constitutive model for frozen sandy soils based on modified Mohr-Coulomb yield criterion. *Chin J Rock Mech Eng.* 37(4):978–986. <https://doi.org/10.13722/j.cnki.jrme.2017.1318>
- Zhang YZ, Zuo SY, Li, Rita YM, Mo YC, Yang GS, Zhang M (2020) Experimental study on the mechanical properties of Guiyang red clay considering the meso micro damage mechanism and stress path. *Scientific Reports*, 10(1), 17449–. <https://doi.org/10.1038/s41598-020-72465-x>
- Zheng SJ, Yao YB, Liu D, Cai YD, Liu Y (2018) Characterizations of full-scale pore size distribution, porosity and permeability of coals: a novel methodology by nuclear magnetic resonance and fractal analysis theory. *Int J Coal Geol* 196 <https://doi.org/10.1016/j.coal.2018.07.008>

Zhu QZ, Yang YH, Lu XQ, Liu DM, Li XW, Zhang QQ, Cai YD (2019) Pore structure of coals by mercury intrusion, N<sub>2</sub> adsorption and NMR: a comparative study. *Appl Sci-Basel.* 9(8). <https://doi.org/10.3390/app9081680>

Zuo SY, Zhang YZ, Pu Q et al (2018) A method for determining the particle size distribution of Guiyang red clay based on laser particle size analyzer. Guizhou: CN108593506A